

光学学报

中红外涡旋激光在有机晶体 DSTMS 中的演化(特邀)

林婷^{1,2}, 孟宪泽², 郑卓锐², 丁菅菅², 宋立伟², 刘一¹, 田野^{2*}

¹ 上海理工大学光电信息与计算机工程学院, 上海 200093;

² 中国科学院上海光学精密机械研究所强场激光物理国家重点实验室, 上海 201800

摘要 具有轨道角动量的涡旋光束相比其他光束有很多独特的性质, 其螺旋状的波前结构和相位变化为诸多应用开辟了新的维度。对涡旋光在非线性有机晶体 DSTMS 中的传输演化机制进行实验研究, 探索了涡旋中红外激光的非线性传输特性, 利用广义高斯光束分解方法模拟分析了拉盖尔-高斯光束经过介质前后的光强分布, 并对比了不同入射涡旋光的偏振态对出射光斑的影响的差异。

关键词 物理光学; 涡旋光束; 五阶非线性; DSTMS 晶体; 偏振

中图分类号 O436

文献标志码 A

DOI: 10.3788/AOS231942

1 引言

涡旋光束^[1]是一种具有轨道角动量(OAM)的光束, 其相位结构呈螺旋分布, 在传播过程中, 中心光强始终保持为0, 同时光束中心相位不确定, 具有相位奇点。涡旋光束因其在空间上的独特性质, 在光镊^[2]、光通信^[3]、光学精密测量^[4]、高精度成像技术^[5]、水下光通信^[6-7]、量子信息处理^[8]、高分辨率显微镜^[9]等领域展现出巨大的应用潜力。在最近十几年, 涡旋光研究及其应用取得了更长足的发展。随着研究中涡旋光功率和能量的显著提升^[10], 对非线性涡旋光现象^[11]如旋转多普勒效应^[12]、基于非线性倍频的模式转换^[13]等的探索吸引了越来越广泛的关注。

拉盖尔-高斯(LG)光束^[14]是一种典型的涡旋光, 拓扑荷数 l 和径向指数 p 是 LG 光束的 2 个基本参数, 故常用 LG_p^l 来描述 LG 光束的基本模式。拓扑荷数 l 影响输出光斑的半径, 径向指数 p 影响光斑“环”的数量。与传统的高斯光束相比, 高阶径向 LG 光束的光强分布更均匀。最近几十年, 研究人员对于 LG 光束在介质中的线性和非线性传输的探索越来越深入, 其涵盖领域也不断拓展, 这为“光学涡旋”发展奠定了坚实的基础。丁攀峰等^[15]基于衍射理论分析了 LG 光束在传输中的光斑和相位变化。Deng 等^[16]结合洛伦兹和高斯公式演变出的四瓣洛伦兹-高斯涡旋光束, 分析了其光束强度和相位的演化规律, 指出随着传输距离的增加, 其四瓣光束的强度分布会被破坏, 由阵列光束

演变为暗空心光束, 相位将变得不规则。Che 等^[17]研究了涡旋场的克尔非线性调制和四波混频涡旋调制。陈欢等^[18]提出一种能够同时实现 LG 光束倍频和模式转换两种功能的光学超晶格, 对不同角向指数的 LG 光束的模式转换过程进行数值模拟, 验证了两种光束模式指数的关系。先期研究大多集中在对涡旋光特性及其线性传输和演化进行分析, 随着研究的深入, 超短脉冲涡旋激光成为研究热点。中红外涡旋激光在驱动高次谐波产生, 获得具有轨道角动量的相干 X 射线方面具有良好的应用前景。由于高次谐波的截止能量与激光波长的平方成正比, 使用更长波长的驱动激光可以产生更高的光子能量。因此, 利用中红外涡旋光产生高次谐波, 有望在紫外到 X 射线波段产生涡旋激光, 为光物理和材料表征领域开辟全新的研究方向。本文通过实验研究了红外涡旋激光在有机晶体 DSTMS (4-N, N-dimethylamino-4'-N'-methyl-stilbazolium 2, 4, 6-trimethylbenzenesulfonate) 中传输时, 由于三阶、五阶非线性效应引起的光束演化过程, 并分析了不同入射光偏振态对横向光场分布的影响。

2 实验研究

2.1 实验装置

实验装置如图 1 所示, 中红外脉冲激光源由一个钛宝石激光器(Astrella, Coherent Inc.)和一个光学参量放大器(OPA)系统组成^[19]。钛宝石激光器输出的 800 nm 脉冲光经过 OPA 后, 发生频率下转换, 产生中

收稿日期: 2023-12-15; 修回日期: 2024-01-19; 录用日期: 2024-01-29; 网络首发日期: 2024-02-20

基金项目: 国家重点研发计划(2022YFA1604401)、国家自然科学基金(12325409, 62105346, 12388102)、上海市基础研究特区项目-中国科学院上海分院

通信作者: *tianye@siom.ac.cn

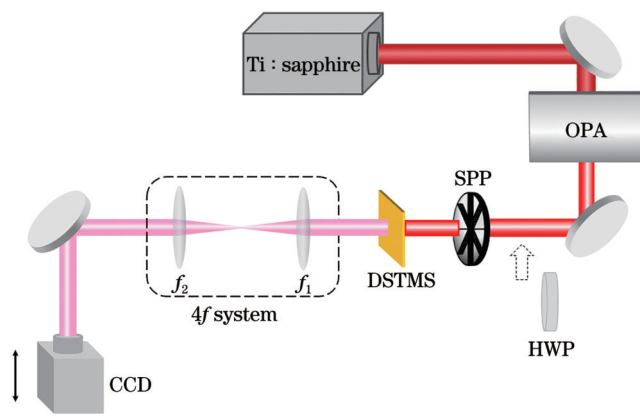


图1 中红外脉冲涡旋光的产生及探测实验装置示意图

Fig. 1 Schematic of the experimental setup for generation and detection of mid-infrared pulsed vortex beam

心波长为1450 nm、脉宽为60 fs、重复频率为1 kHz的中红外激光。经过定制的螺旋相位板(SPP)后,中红外激光被调制为LG激光并垂直入射到厚度为640 μm的有机晶体表面。利用两个透镜搭建4f成像系统来对晶体内垂直于光传播方向的任一平面内的光斑成像,其中 $f_1=f_2=10\text{ cm}$ 。在水平方向上前后移动CCD相机,从晶体后表面处开始观察并记录LG激光在传播过程中的光斑演化。

OPA系统输出的中红外激光入射到螺旋相位板,产生能量为20 μJ、拓扑荷数为1的LG₀¹涡旋光束。螺旋相位板的材质为石英(JGS1),在1.45 μm波长处的折射率为1.4456。螺旋相位板的最大厚度为3 mm,阶

梯高度为3.253 μm。由于螺旋相位板表面为连续型,因此其产生的LG激光相位变化也是连续的。有机晶体DSTMS在红外波段有很大的二阶非线性系数 d [(214±20) pm/V]和电光系数 γ [(37±3) pm/V],且各向异性较强,在超短脉冲激光驱动下能够产生很强的非线性效应,包括光整流效应、倍频效应、克尔效应等^[20]。

2.2 实验结果与分析

实验中测量中红外LG激光经过DSTMS晶体前后的光斑变化,并与BBO晶体的光斑进行对比,以分析LG激光经过不同晶体后的光斑特性。图2(a)~(c)展示了中红外LG激光的初始光斑和分别经过BBO、DSTMS晶体后的光斑。为了便于分析,以光斑中心点所在的横轴为x轴,光强为y轴,可以得到图2(d)中关于中红外LG激光经过不同晶体后的光强分布。可以看出,经过BBO晶体后,光斑中的亮环仍然只有1个,光斑半径几乎没有发生改变。在图2(a)、(b)中,最亮环的外围还有微弱的次亮环,由于钛宝石激光器的输出光为超短脉冲激光,经OPA频率下转换后,产生宽带中红外超短脉冲激光。超短脉冲激光经过SPP后,生成的涡旋光束OAM模式较为复杂,使其在光斑形状上与标准LG激光有所差异。进一步地,红外涡旋光经过DSTMS晶体后,其光斑发生明显变化,由原来的甜甜圈结构变成了3圈极细的亮环,光环数量增多。从图2(d)可以看出,整体光斑直径从6 mm减小至4 mm,中心亮环的直径由2 mm减小至0.5 mm,中心亮环直径大幅度减小。

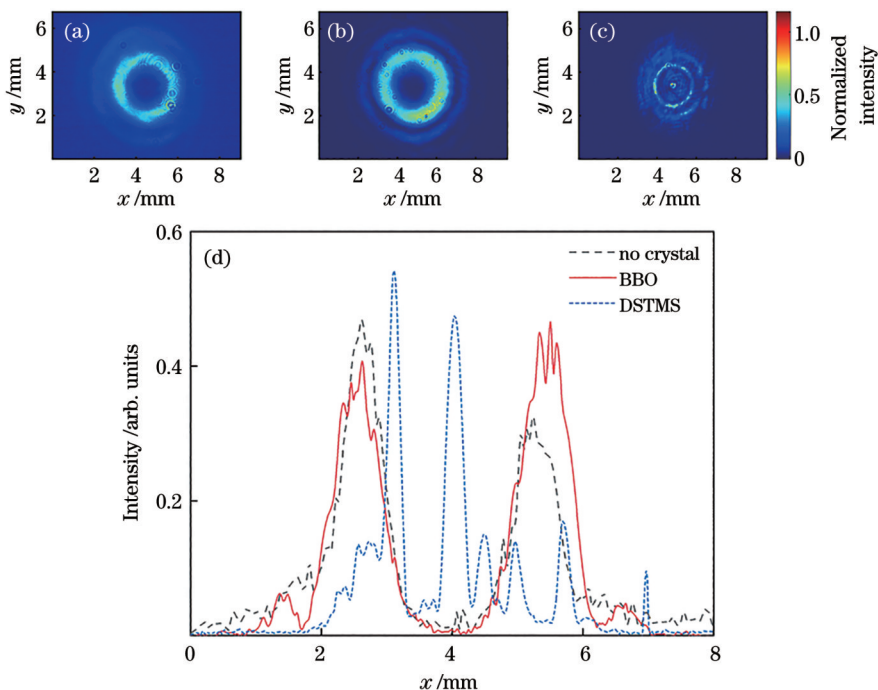


图2 中红外涡旋光经过不同晶体后的光斑对比。(a)无晶体;(b)BBO;(c)DSTMS;

Fig. 2 Comparison of beam spots of mid-IR vortex beam passing through different crystals. (a) No crystal; (b) BBO; (c) DSTMS; (d) intensity distribution along x axis at the center of vortex beam

DSTMS晶体对泵浦光存在三光子吸收的非线性过程,这说明当涡旋光在晶体中发生强非线性效应时,其光束特性将受到显著影响。当泵浦光的偏振方向旋转到晶体非线性最强的方向时,DSTMS的非线性折射率系数主要由级联二阶光整流过程和线性电光效应相结合产生的准三阶非线性折射率系数主导^[21]。其附加非线性折射率会导致泵浦光的折射率随光强变化,进而导致光谱展宽。对于入射LG光束在克尔介质中发生光谱展宽后产生的各频谱分量,其各自对应的LG模式都具有相同的拓扑荷数和径向指数。各频谱分量的频率值不同,导致各自对应的瑞利长度和光腰位置不同,而频谱分量对应的LG涡旋光的光场表达式不同,所对应的亮环半径不同。

如果在给定波长下只有一种多光子吸收占主导地位,那么光强 $I(z, R, t)$ 的表达式^[22]为

$$\frac{dI(z, R, t)}{dz} = -\alpha_N I^N(z, R, t), \quad (1)$$

式中: z 为传播距离; R 为横坐标; t 为时间; α_N 为 N 个光子的吸收系数。

介质中的非线性效应与非线性折射率有关,介质折射率 n 与入射光强 I 的关系^[23]为

$$n = n_0 + n_2 I + n_4 I^2 + \dots, \quad (2)$$

式中: n_0 为介质的线性折射率; n_2 和 n_4 分别为三阶、五阶非线性折射率系数。

在具有较大二阶极化率 $\chi^{(2)}$ 的非中心对称晶体(如DSTMS晶体)中,非线性折射率由以下三部分组成^[24],即

$$n^{\text{total}} = n^{\text{direct}} + n^{\text{SHG}} + n^{\text{OR}}, \quad (3)$$

式中: $n^{\text{direct}} \propto \text{Re}\{\chi^{(3)}\}$ 表示由其内禀的三阶非线性极化率 $\chi^{(3)}$ 所引起的非线性折射率; $n^{\text{SHG}} \propto d_{\text{eff}}^2 / \Delta k$ 表示由二阶级联过程对二次谐波所引起的非线性折射率, d_{eff} 为有效非线性光学系数, $\Delta k = k^{2\omega} - k^\omega$ 为波矢失配; $n^{\text{OR}} \propto r_{\text{ik}}^2$ 表示由级联二阶光整流过程和线性电光效应相结合产生的非线性折射率, r_{ik} 为电光系数。当入射飞秒脉冲沿[001]轴传播时,对于二次谐波产生,I型和II型的相位匹配相差太大,因此 n^{SHG} 可以忽略不计。此外,[100]光偏振符合太赫兹波产生的最佳条件,因此 n^{OR} 对沿[100]方向的偏振的贡献最大,它与方位角 θ 成 $\cos^4 \theta$ 关系。因此,DSTMS的非线性折射率 n_2 与方位角 θ 的函数关系^[25]可以表示为

$$n^{\text{total}} \propto a_1 \cos^4 \theta + a_2 \sin^4 \theta + a_3 \frac{\sin^2 \theta}{4}, \quad (4)$$

$$a_1 = \text{Re}\{\chi_{1111}^{(3)}\} + n^{\text{OR}}, \quad (5)$$

式中: a_1 为[100]轴的本征 $\chi^{(3)}$ 对角张量分量和 n^{OR} 的总和; a_2 和 a_3 分别为[010]轴的本征 $\chi^{(3)}$ 对角张量分量和非对角分量。

Li等^[21]研究了DSTMS晶体在波长为1.43 μm的飞秒脉冲激发下的光学克尔非线性和多光子特性,采用Z扫描法测量了在该波长处DSTMS晶体的非线性

折射率和多光子吸收系数。通过测量不同方位角下全开孔径(OA)和半闭合孔径(CA)的归一化透射率并且对其进行拟合,可以得到三光子吸收系数 α_4 和非线性折射率 n_2 与方位角 θ 的函数关系。实验结果表明,多光子吸收和光学克尔非线性都具有很强的各向异性。当电场偏振从[100]旋转到[010]时, α_4 的值从 $(6.02 \pm 0.51) \times 10^{-2} \text{ cm}^3/\text{GW}^2$ 变为接近于 $0[(0.01 \pm 0.14) \times 10^{-2} \text{ cm}^3/\text{GW}^2]$, n_2 的值从 $(2.19 \pm 0.28) \times 10^{-5} \text{ cm}^2/\text{GW}$ 变为 $(0.08 \pm 0.34) \times 10^{-5} \text{ cm}^2/\text{GW}$ 。式(4)中,后两项的值近乎为0,而 a_1 的值为 $(2.13 \pm 0.37) \times 10^{-5} \text{ cm}^2/\text{GW}$,即DSTMS晶体的非线性折射率系数主要由级联二阶光整流过程和线性电光效应相结合产生的准三阶非线性折射率系数主导,而其自身的三阶非线性折射率系数非常小,且其在1.43 μm波长处的多光子吸收中三光子吸收占主导地位。三光子吸收本质上是一个五阶非线性过程,当传输功率较大或介质的五阶非线性折射率系数较高时,需要考虑五阶非线性效应对光脉冲传输特性的影响。Chen等^[26]使用变分法理论分析了LG光束在三阶、五阶非线性介质中的传播特性。当低强度的光束在三阶、五阶介质中传播时,用变分法模拟LG光束光强的空间分布。模拟得到LG光束在经过纯三阶非线性介质和三阶、五阶非线性介质之后的远场横向强度分布。当三阶非线性介质位于束腰($z_{\text{in}}=0$)处时,LG光束穿过三阶非线性介质后的远场横向分布与穿过线性介质后的远场横向分布相同。然而,当将三阶、五阶非线性介质置于光腰处时,LG光束的远场横向分布与穿过线性介质后的远场横向分布相比呈现出显著差异。若三阶非线性介质位于束腰后($z_{\text{in}}>0$),LG光束穿过三阶非线性介质后的远场强度分布和穿过线性介质后的强度相比被压缩。当非线性介质具有三阶、五阶非线性且五阶非线性折射率系数为负时,LG光束则被扩展。这与在三阶非线性介质中的行为相反。然而,相比于三阶非线性折射率系数和光强,LG光束在三阶、五阶非线性介质中的传播行为在很大程度上取决于五阶非线性折射率系数的大小和符号。随着负五阶非线性效应的增强,其作用从三阶非线性效应为主转变为五阶非线性效应为主。这证实了红外LG激光在有机晶体DSTMS中传输后,三阶、五阶非线性效应引起了光束演化。

为了验证上述光斑演化过程,通过MATLAB软件进行仿真分析,基于广义高斯光束分解方法^[27],可以模拟出经过具有类克尔效应的DSTMS介质前后的LG光束的光场分布,仿真结果如图3所示。在计算中波长取1.45 μm,束腰半径 ω_0 为3.5 mm,取样点数为1000。

LG_0^1 光束垂直入射到具有类克尔效应的DSTMS晶体后,根据文献^[28],考虑到薄光学克尔介质对LG光束的影响,对光场进行泰勒级数展开并忽略高阶项,从DSTMS晶体出射后电场 E' 可表示为

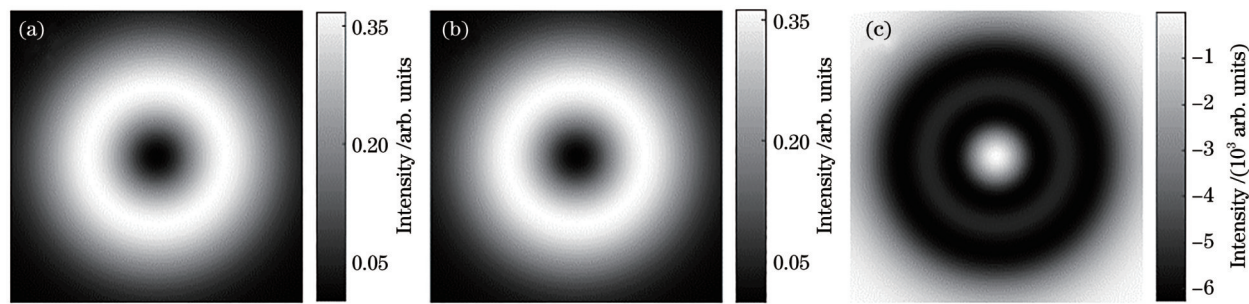


图3 经过具有类克尔效应的DSTMS前后的LG光束的光强分布仿真结果。(a)入射DSTMS晶体之前的 LG_0^1 光束的光强分布;(b)根据文献[28]计算得到的从DSTMS晶体出射的光束光强分布;(c)出射光与入射光的光强之差

Fig. 3 Simulation results of light intensity distribution of LG beams incident on and exiting DSTMS with Kerr-like effect. (a) Light intensity distribution of LG_0^1 beam incident on the DSTMS crystal; (b) intensity distribution of the beam emitted from DSTMS crystal calculated according to Ref. [28]; (c) intensity difference between the outgoing light and the incident light

$$E'(r, \phi, z) \approx F_{0,0} LG_0^1(r, \phi, z; z_R) + \frac{2}{3\sqrt{3}} F_{0,1} LG_0^1(r, \phi, z - z_{w1}; z_{R1}) - \frac{1}{3\sqrt{3}} F_{1,1} LG_1^1(r, \phi, z - z_{w1}; z_{R1}), \quad (6)$$

$$F_{p,m} = E_0 \exp(-\alpha d/2) \frac{(-i\Delta\Phi_0)^m}{m!(2m+1)} \sqrt{\frac{(2m+1)^2 + Z^2}{(1+Z^2)^{2m+1}}} \times \exp\left[-ikz_R \frac{4m(m+1)Z}{Z^2 + (2m+1)^2}\right] \times \\ \exp\left[i(2p_0 + |l_0| + 1)\arctan(Z)\right] \times \exp\left[-i(2p + |l_0| + 1)\arctan\left(\frac{Z}{2m+1}\right)\right], \quad (7)$$

式中: $Z = z_s/z_R$, $z_R = k\omega_0^2/2$ 为瑞利长度; ω_0 为束腰半径; α 为线性吸收系数; $\Delta\Phi_0$ 表示与焦点处($z_s = 0$)的最大非线性相位变化 $\Delta\Phi_{\max}(z_s)$ 成正比的常数。用 $C \times LG_p^l(r, \phi, z - z_w; z_R)$ 来明确描述LG光束,其中 l 为角模态数, p 为横向径向模态数, z_w 为 z 轴上的光腰位置, C 为给出振幅和初始相位的复常数。输出光场包括产生的 LG_0^1 和 LG_1^1 光束,光强分布如图3(b)所示。从图3(c)可以看出,克尔介质对入射LG光束的影响是产生不同径向模式的LG光束。

实验进一步研究了入射LG光束偏振态对晶体后表面出射光斑的影响,图4(a)~(f)所示为入射光的偏振态发生变化时,DSTMS晶体后表面出射光的光斑演化情况。以光斑中心为圆心,对与圆心距离相同的点的光强进行积分,可以得到图4(g)所示的不同入射LG光束偏振态下出射光的光强分布。

入射中红外光的初始偏振态是 p 偏振。实验中,通过在螺旋相位板前加入1450 nm的半波片(HWP)来改变入射光的偏振态。固定CCD的位置以及DSTMS晶体的角度,将半波片从初始位置旋转90°,即旋转角度从0°变化到90°,可以将入射光的偏振方向从初始位置0°连续旋转180°。实验发现:当半波片的旋转角度为0°和90°(对应偏振不发生改变)时,光斑中出现最多亮环(3个)。随着旋转角度的改变,亮环数量逐渐减少;当半波片的旋转角度为15°和75°(即偏振方向改变30°)时,亮环数量为2个,且中心亮环几乎消失;当半波片的旋转角度为30°、60°(即偏振方向改变60°)和45°(即偏振方向改变90°)时,整个光斑呈现出

类似于甜甜圈的结构,光斑直径发生微弱变化;当半波片旋转角为30°时,光斑直径为2.9 mm;当半波片旋转角为45°时,光斑直径为2.7 mm;当半波片旋转角为60°时,光斑直径为2.52 mm。从图4(g)可以看出,整体光斑直径几乎没有发生变化,中心亮环的直径由0.24 mm大幅增加至2.44 mm。改变入射涡旋光的偏振态,非线性效应随之变化,从而导致不同入射涡旋光的偏振态下出射光的光强分布不同。当泵浦光的偏振方向旋转到晶体非线性最强的方向时,DSTMS晶体的非线性折射率系数主要由级联二阶光整流过程和线性电光效应相结合产生的准三阶非线性折射率系数主导^[21]。在对与光斑中心距离相同的点的光强进行积分得到的出射光的光强分布中,当半波片的旋转角度为0°和90°(对应的偏振方向为晶体光轴方向)时,非线性效应最强。以上实验结果说明,不同偏振态的入射光会产生不同光强分布的LG光束,进一步证实了非线性过程对涡旋光束特性的影响。

3 结 论

对LG光束在太赫兹有机晶体DSTMS中的演化机制进行实验研究,结果表明非线性传输效应能够在很大程度上改变LG光束的光强分布。利用广义高斯光束分解方法对LG光束经过具有类克尔效应的介质前后的光强分布进行仿真分析,发现克尔介质对入射LG光束的影响是产生不同径向模式的LG光束。此外,研究了不同入射LG光束的偏振态对LG中红外激光在非线性介质DSTMS晶体中传输的影响,展示了

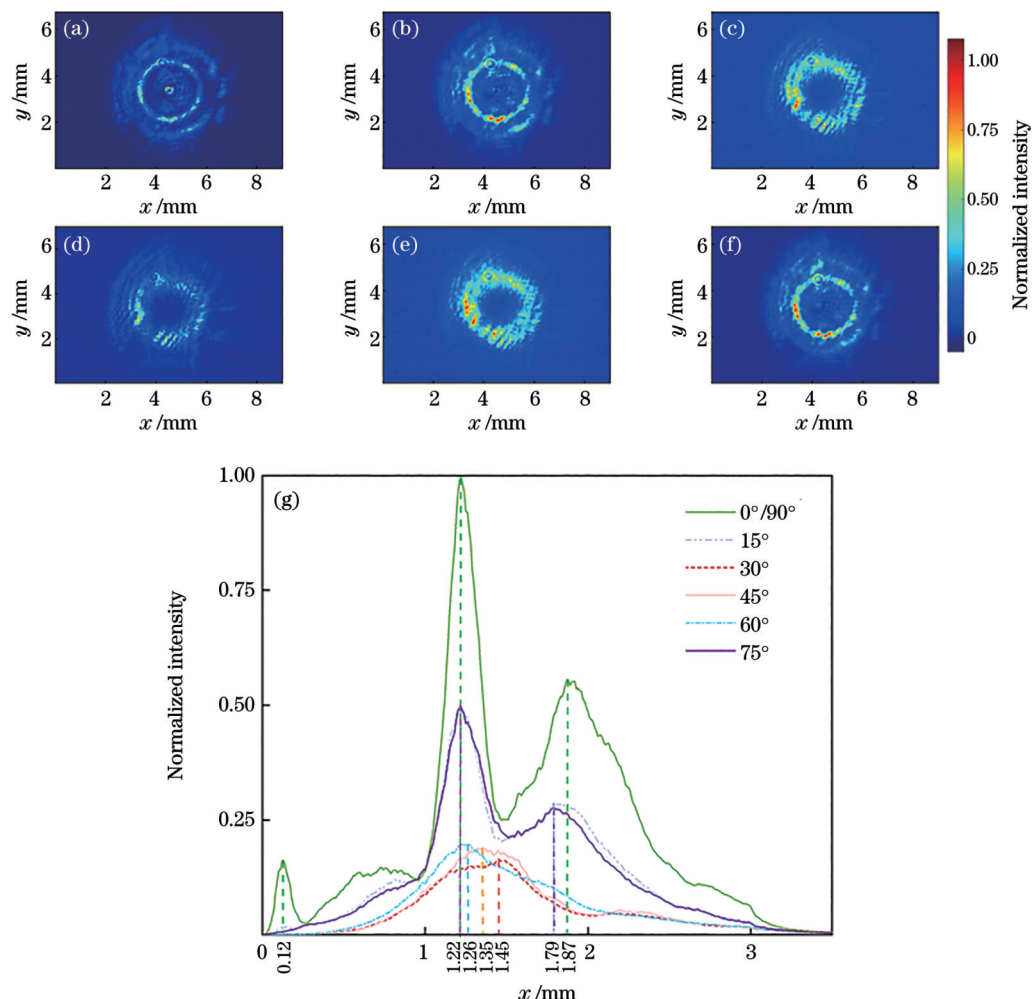


图4 入射涡旋光的偏振态对出射光斑强度分布的影响。偏振方向为(a) $0^\circ/90^\circ$ 、(b) 15° 、(c) 30° 、(d) 45° 、(e) 60° 、(f) 75° 时的光斑；(g)驱动激光偏振方向为 $0^\circ\sim90^\circ$ 时的光斑径向强度分布

Fig. 4 Influence of polarization state of incoming vortex beam on intensity distribution of outgoing beam. Light spots under polarization direction of (a) $0^\circ/90^\circ$, (b) 15° , (c) 30° , (d) 45° , (e) 60° , and (f) 75° ; (g) radial intensity distribution of the corresponding spots when the driving laser polarization is $0^\circ\sim90^\circ$

非线性传输对 LG 光束的影响。

参 考 文 献

- [1] Fang L, Padgett M J, Wang J. Sharing a common origin between the rotational and linear Doppler effects[J]. *Laser & Photonics Reviews*, 2017, 11(6): 1770064.
- [2] Zhang D W, Yuan X C. Optical doughnut for optical tweezers [J]. *Optics Letters*, 2003, 28(9): 740-742.
- [3] Gibson G, Courtial J, Padgett M, et al. Free-space information transfer using light beams carrying orbital angular momentum[J]. *Optics Express*, 2004, 12(22): 5448-5456.
- [4] Phillips D B, Lee M P, Speirs F C, et al. Rotational Doppler velocimetry to probe the angular velocity of spinning microparticles[J]. *Physical Review A*, 2014, 90(1): 011801.
- [5] Rui G H, Wang X Y, Cui Y P. Manipulation of metallic nanoparticle with evanescent vortex Bessel beam[J]. *Optics Express*, 2015, 23(20): 25707-25716.
- [6] 韦育, 于永河, 黑小兵, 等. 涡旋光束和光子计数在水下光通信中的应用[J]. 激光与光电子学进展, 2022, 59(13): 1301001. Wei Y, Yu Y H, Hei X B, et al. Application of vortex beam and photon counting in underwater optical communication[J]. *Laser & Optoelectronics Progress*, 2022, 59(13): 1301001.
- [7] 王明军, 余文辉, 黄朝军. 水下拉盖尔-高斯涡旋光束及其叠加态传输特性[J]. *光学学报*, 2023, 43(6): 0626001. Wang M J, Yu W H, Huang C J. Transmission characteristics of underwater Laguerre-Gaussian vortex beam and its superposition states[J]. *Acta Optica Sinica*, 2023, 43(6): 0626001.
- [8] Lavery M P J, Robertson D J, Sponselli A, et al. Efficient measurement of an optical orbital-angular-momentum spectrum comprising more than 50 states[J]. *New Journal of Physics*, 2013, 15(1): 013024.
- [9] Westphal V, Hell S W. Nanoscale resolution in the focal plane of an optical microscope[J]. *Physical Review Letters*, 2005, 94(14): 143903.
- [10] Vieira J, Trines R M G M, Alves E P, et al. Amplification and generation of ultra-intense twisted laser pulses via stimulated Raman scattering[J]. *Nature Communications*, 2016, 7: 10371.
- [11] Gauthier D, Ribić P R, Adhikary G, et al. Tunable orbital angular momentum in high-harmonic generation[J]. *Nature Communications*, 2017, 8: 14971.
- [12] Li G X, Zentgraf T, Zhang S. Rotational Doppler effect in nonlinear optics[J]. *Nature Physics*, 2016, 12: 736-740.
- [13] 陈顺意, 丁攀峰, 蒲继雄. 离轴涡旋光束弱走离条件下的倍频效应[J]. *物理学报*, 2015, 64(24): 244204.

- Chen S Y, Ding P F, Pu J X. Frequency doubling effect of off-axial vortex beam in the case of weak walk-off[J]. Acta Physica Sinica, 2015, 64(24): 244204.
- [14] Allen L, Beijersbergen M W, Spreeuw R J, et al. Orbital angular momentum of light and the transformation of Laguerre-Gaussian laser modes[J]. Physical Review A, 1992, 45(11): 8185-8189.
- [15] 丁攀峰, 蒲继雄. 拉盖尔高斯涡旋光束的传输[J]. 物理学报, 2011, 60(9): 094204.
- Ding P F, Pu J X. Propagation of Laguerre-Gaussian vortex beam[J]. Acta Physica Sinica, 2011, 60(9): 094204.
- [16] Deng W T, Zhao G, Xia H J, et al. Four-petal Lorentz-Gauss vortex beam and its propagation in free space[J]. Optik, 2020, 202: 163586.
- [17] Che J L, Zhao P L, Ma D M, et al. Kerr-nonlinearity-modulated dressed vortex four-wave mixing from photonic band gap[J]. Optics Express, 2020, 28(12): 18343-18350.
- [18] 陈欢, 吴淦, 孙旭辉, 等. 基于局域相位匹配的特殊光束非线性模式转换[J]. 光学学报, 2023, 43(14): 1419001.
- Chen H, Wu G, Sun X H, et al. Nonlinear mode conversion of special beams based on local quasi-phase-matching[J]. Acta Optica Sinica, 2023, 43(14): 1419001.
- [19] Wang P F, Shao B J, Su H P, et al. High-repetition-rate, high-peak-power 1450 nm laser source based on optical parametric chirped pulse amplification[J]. High Power Laser Science and Engineering, 2019, 7: e32.
- [20] Meng X Z, Wang K, Yu X Q, et al. Generation and characterization of intense terahertz pulses from DSTMS crystal [J]. Optics Express, 2023, 31(15): 23923-23930.
- [21] Li J, Rana R, Zhu L G, et al. Optical Kerr nonlinearity and multiphoton absorption of DSTMS measured by the Z-scan method[J]. Journal of the Optical Society of America B, 2021, 38(9): 2511-2516.
- [22] Hurlbut W C, Lee Y S, Vodopyanov K L, et al. Multiphoton absorption and nonlinear refraction of GaAs in the mid-infrared [J]. Optics Letters, 2007, 32(6): 668-670.
- [23] Choudhuri A, Porsezian K. Dark-in-the-Bright solitary wave solution of higher-order nonlinear Schrödinger equation with non-Kerr terms[J]. Optics Communications, 2012, 285(3): 364-367.
- [24] Bosshard C, Spreiter R, Zgonik M, et al. Kerr nonlinearity via cascaded optical rectification and the linear electro-optic effect[J]. Physical Review Letters, 1995, 74(14): 2816-2819.
- [25] Desalvo R, Sheik-Bahae M, Said A A, et al. Z-scan measurements of the anisotropy of nonlinear refraction and absorption in crystals[J]. Optics Letters, 1993, 18(3): 194-196.
- [26] Chen R P, Wang H T. Propagation of Laguerre-Gaussian beams in cubic-quintic nonlinear media by variational approach[J]. Optics & Laser Technology, 2010, 42(8): 1318-1322.
- [27] Sheik-Bahae M, Said A A, Wei T H, et al. Sensitive measurement of optical nonlinearities using a single beam[J]. IEEE Journal of Quantum Electronics, 1990, 26(4): 760-769.
- [28] Zhang W Y, Kuzyk M G. Effect of a thin optical Kerr medium on a Laguerre-Gaussian beam[J]. Applied Physics Letters, 2006, 89(10): 101103.

Evolution of Mid-Infrared Vortex Laser in Organic Crystal DSTMS (Invited)

Lin Ting^{1,2}, Meng Xianze², Zheng Zhuorui², Ding Yingying², Song Liwei², Liu Yi¹, Tian Ye^{2*}

¹College of Optical-Electrical and Computer Engineering, University of Shanghai for Science and Technology, Shanghai 200093, China;

²State Key Laboratory of High Field Laser Physics, Shanghai Institute of Optics and Fine Mechanics, Chinese Academy of Sciences, Shanghai 201800, China

Abstract

Objective Vortex beams with orbital angular momentum (OAM) have many unique properties compared to other beams, and their spiral wavefront structure and phase changes open up new dimensions for applications such as lithography, optical communication, optical trapping, and quantum entanglement. In recent decades, researchers have been exploring the linear and nonlinear transmission of the Laguerre-Gaussian (LG) vortex beam in media, and the coverage has been continuously expanded, which lays a solid foundation for developing the optical vortex. Most relevant research focuses on analyzing the properties of vortex beams and their linear transmission and evolution. However, the ultrashort pulse vortex laser has become a research hotspot with extensive studies. Since the inclusion of nonlinear processes will greatly increase the complexity of vortex beam analysis, the study on transmission and evolution of ultrashort pulse vortex lasers in nonlinear media is still rare. Thus, we experimentally investigate the propagation of mid-infrared LG beams in organic crystal DSTMS due to the cubic-quintic nonlinear effect and analyze the differences in the effect of polarization of the incident vortex beam on the transverse light field distribution.

Methods High power mid-infrared optical parametric amplifier (OPA) pulses with 1450 nm center wavelength, 60 fs pulse duration, and 1 kHz repetition rate serve as the pump of the system. After passing through a customized spiral phase plate (SPP), the mid-infrared laser light is modulated into vortex beams and incident perpendicularly onto the surface of an organic crystal with a 640 μm thickness. A 4f imaging system is constructed using two lenses to conduct imaging on the spot in either plane perpendicular to the light propagation direction within the crystal. The CCD camera moves back and forth in the horizontal direction to observe and record the spot evolution of the vortex beam during propagation, starting

from the rear surface of the crystal.

Results and Discussions In the experiment, the spot changes of mid-infrared vortex light before and after passing through the DSTMS crystal are found and compared with those of the BBO crystal to analyze the spot characteristics of the vortex beam after passing through different crystals. After passing through the BBO crystal, there is still only one bright ring in the spot, with the spot radius almost unchanged. However, after passing through the DSTMS crystal, the spot changes significantly from the original doughnut structure to three thin bright rings, and the number of rings increases. This is due to the nonlinear process of three-photon absorption of pump light by the DSTMS crystal. When the pump light polarization fulfills the optimal THz generation conditions, the nonlinear refractive index of DSTMS mainly originates from the quasi- $\chi^{(3)}$ effect due to a combination of the cascaded 2nd-order OR process and the linear EO effect. The contribution from the intrinsic $\chi^{(3)}$ nonlinearity of DSTMS should be negligible. Its additional nonlinear refractive index causes the refractive index of the pump light to vary with light intensity, which in turn leads to spectrum broadening. For each spectral component generated after the spectrum broadening of the incident LG beam in the Kerr medium, its respective corresponding LG mode has the same topological charge and radial index. As the frequency value of each spectral component is different, the respective corresponding Rayleigh length and beam waist position are different to bring various light field expressions for the LG vortex beam corresponding to each spectral component. Therefore, the corresponding brightest rings have different radii, and each bright ring generally does not coincide with each other in the observation plane, resulting in a weak spot intensity in most regions of the observation plane. To verify the above optical spot evolution process, we can simulate the light field distribution of the LG beam before and after passing through the DSTMS medium with a Kerr-like effect by MATLAB simulation analysis based on the generalized Gaussian beam decomposition method, with the simulation results shown in Fig. 3. Fig. 3(c) reveals that the effect of the Kerr medium on the incident LG beam is to produce LG beams with different radial modes. Meanwhile, the effect of the polarization of the incident vortex light on the spot of the outgoing light from the rear surface of the crystal is further investigated experimentally, and the experimental results illustrate that the incident light with different polarization produces vortex beams with different light intensity distributions.

Conclusions We research the evolutionary mechanism of vortex beams in nonlinear organic crystal DSTMS initially, showing that the nonlinear transmission effect can change the light intensity distribution of vortex beams to a large extent. The generalized Gaussian beam decomposition method is utilized to simulate and analyze the light intensity distribution of the LG beam before and after passing through the medium with a Kerr-like effect, which indicates that the Kerr medium affects the incident LG beam by producing LG beams with different radial modes. Additionally, the effect of different polarization of the incident vortex light on vortex mid-infrared laser transmission in DSTMS is studied to demonstrate the effect of nonlinear transmission on the LG beam.

Key words physical optics; vortex beam; fifth-order nonlinearity; DSTMS crystal; polarization